Earth and Planetary Science Letters 497 (2018) 22–28

Contents lists available at ScienceDirect

Earth and Planetary Science Letters

www.elsevier.com/locate/epsl

Exponentially decreasing erosion rates protect the high-elevation crests of the Himalaya

Argha Banerjee *, Bilal Ahmad Wani

Earth and Climate Science, IISER, Pune, India

ARTICLE INFO

Article history:
Received 10 January 2018
Received in revised form 27 May 2018
Accepted 3 June 2018
Available online xxxx
Editor: J.-P. Avouac

Keywords:
debris-covered glaciers
headwall erosion
frost-cracking
Himalayan topography

ABSTRACT

Glacierised mountains erode rapidly due to efficient glacial erosion around the long-term equilibrium line altitude (ELA), as well as by intense frost-cracking action. This 'glacial buzzsaw' is hypothesised to limit mountain heights globally to within about 1.5 km of the local ELA. However, we show that the high Himalaya contrasts this picture with a precipitous decline in the erosion rate at its high-elevation crests. We obtain headwall-erosion rates at eight Himalayan debris-covered glaciers from estimates of the corresponding supraglacial debris flux. The data reveal large variation of erosion rates in the range of 0.04–1.0 mm/yr. We establish that this variability is controlled by an exponential decrease in erosion rate with decreasing mean annual temperature of the headwall due to a decline in frost-cracking intensity at low temperatures. The implied order of magnitude decline of erosion rate at the high altitude of the Himalaya, apart from the pattern and magnitude of uplift, may be crucial for generating relief, and for protecting the spectacularly high crests from the action of 'glacial buzzsaw'.

© 2018 Elsevier B.V. All rights reserved.

1. Introduction

The elevation of a mountain belt is determined by an interplay between uplift and erosion (Beaumont et al., 1992; Montgomery, 1994; Montgomery et al., 2001). Long-term uplift triggers climatic and geomorphic feedbacks that strengthen fluvial and/or glacial erosion and hillslope processes, and limit the maximum elevation and relief (Whipple and Tucker, 1999; Anders et al., 2008; Molnar et al., 2010). It is known that either fluvial or glacial erosion, or a combination of both (Brozović et al., 1997; Lavé and Avouac, 2001; Gabet et al., 2008; Koppes and Montgomery, 2009) keep pace with relatively rapid uplift in young mountain belts like the Himalaya. Rapid physical weathering of rock by frost-cracking helps maintain a high erosion rate in such glacierised landscapes (Hales and Roering, 2005, 2007; Delunel et al., 2010; Anderson et al., 2013; Scherler, 2014). It has been argued that the 'glacial buzzsaw' – efficient erosion around the long-term glacier ELA – erodes mountain belts rapidly, limiting the peak elevation to within 1500 m of the ELA (Brozović et al., 1997; Montgomery et al., 2001; Egholm et al., 2009). Given these processes, the spectacular height of the crests of the Himalaya is quite intriguing. Some clues to this puzzle may lie in the control of relevant climatic and morphological parameters on erosional processes in these top-of-the-world landscapes. However, erosion rate measurements at these inaccessible rugged glacierised landscapes are scant (Heimsath and McGlynn, 2008; Barker, 2016) and the variability of local erosion rates with climatic and morphological factors remain largely unexplored. The strong variability of some of these factors over relatively small horizontal distances in the region further complicates the matter.

Here, we attempt a first-order quantification of headwall erosion rates at several glacial valleys in the high Himalaya, making use of existing data of supraglacial debris thickness (Nakawo, 1979; Heimsath and McGlynn, 2008; Rounce and McKinney, 2014; Schauwecker et al., 2015) and ice-surface velocities from six Himalayan glaciers (Nakawo et al., 1976; Heimsath and McGlynn, 2008; Scherler et al., 2011a, 2011b), complemented by our field data of debris-thickness distribution from two more Himalayan glaciers. We compute supraglacial-debris flux and the corresponding headwall erosion rate for each of these eight glaciers that are spread across the central and western Himalaya. The role of climatic and morphological factors, including that of frost-cracking, in controlling the observed variation of erosion rates is investigated.

2. Supraglacial debris cover in the Himalaya

High-relief Himalayan glacial valleys are often characterised by very steep and high headwalls. Weathering of these headwalls supplies significant debris load to the glaciers (Nakawo et al., 1986; Benn and Lehmkuhl, 2000; Benn et al., 2003; Scherler et al., 2011a; Nagai et al., 2013). The abundant debris supply usually

* Corresponding author.
E-mail address: argha@iiserpune.ac.in (A. Banerjee).

https://doi.org/10.1016/j.epsl.2018.06.001
0012-821X/© 2018 Elsevier B.V. All rights reserved.

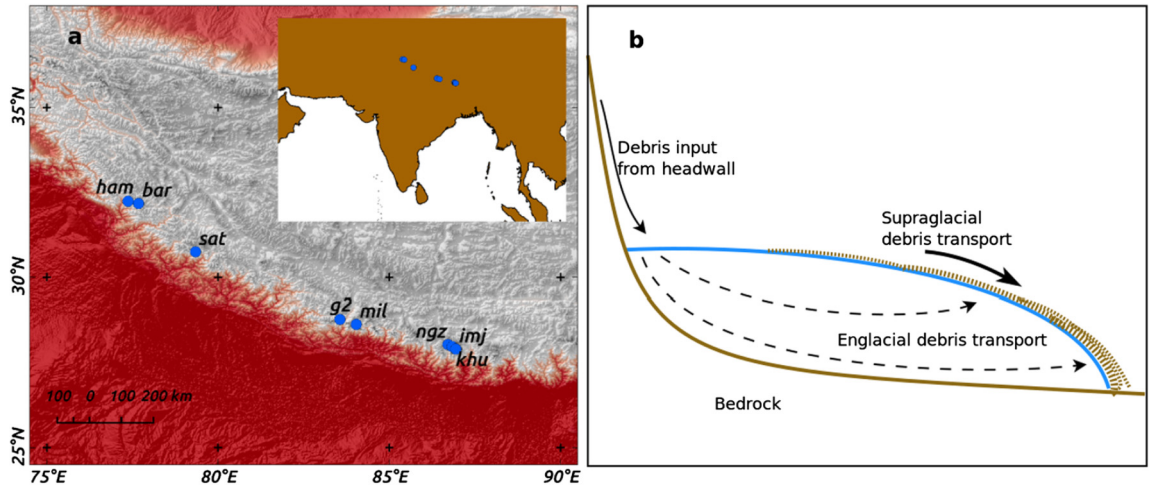

Fig. 1. (a) Locations of the eight debris-covered Himalayan glaciers that are studied here (see text for glacier names. Various other details about the glaciers are given in Table S1). Inset shows locations of the glaciers on a large scale map. (b) A schematic diagram of a typical debris-covered Himalayan glacier with steep headwall (after Anderson and Anderson, 2016), showing the supraglacial and englacial transport of debris sourced from the eroding headwall.

leads to widespread supraglacial debris mantles over the ablation zone of Himalayan glaciers that could be up to a couple of meters thick (Nakawo, 1979; Nakawo et al., 1986; Heimsath and McGlynn, 2008; McCarthy et al., 2017; Nicholson and Mertes, 2017) (Fig. 1b). The magnitude of the flux of supraglacial debris being transported down-valley by these glaciers can be utilised to estimate the rate of erosion of the corresponding headwall (Heimsath and McGlynn, 2008), under the assumptions of 1) an efficient transport of the eroded material from the steep slopes on to the glacier via rockfall and avalanches, and 2) a steady-state condition of the debris-ice coupled system (Heimsath and McGlynn, 2008).

Apart from its geomorphic role discussed above, the supraglacial debris layer, when thicker than a few cm, provides insulation to the underlying ice surface and inhibits melt (Östrem, 1959). This alters the mass balance-elevation relationship and leads to a dramatically different climatic response: a rapidly warming climate does not cause any immediate length retreat for a debris-covered glacier. Instead, the glacier loses mass by thinning and stagnation of the tongue (Scherler et al., 2011b; Banerjee and Shankar, 2013). The peculiar climatic response of debris-covered glaciers and their abundance in the Himalaya have motivated a large body of recent work on various aspects of this type of glacier. In particular, quite a few of these studies focused on measurement of the supraglacial debris-thickness distribution, either by direct field surveys (McCarthy et al., 2017; Nicholson and Mertes, 2017) or by using energy-balance models applied to thermal-band remote-sensing data (Rounce and McKinney, 2014; Schauwecker et al., 2015). On the other hand, image-correlation based feature-tracking techniques applied to repeat satellite images (Scherler et al., 2008; Quincey et al., 2009) have allowed access to spatial pattern of multi-annual surface velocities for hundreds of glaciers across the Himalaya (Scherler et al., 2011b). Such data can easily be exploited to obtain the supraglacial debris flux in the respective glaciers.

3. Methods

Data necessary for calculating debris-flux are available for eight glaciers spread across the central and western Himalaya. These are Imja–Lhotse–Shar (Imj), Khumbu (Khu), Ngzompa (Ngz), Milerapa's (Mil), G2 (G2), Satopanth (Sat), Bara Shigri (Bar) and Hamtah (Ham) Glaciers. These glaciers have total areas in the range of 0.8–102 km^2 and headwall areas in the range of 0.6–65 km^2. The locations of these glaciers are shown in Fig. 1a, and various other relevant details are listed in Table S1.

Headwalls for each of the glaciers, excluding the portions that are ice covered, were delineated using Google-Earth. Parts of the sidewall that are not separated from the glacier by lateral moraines were also included in the debris-source area. The total debris-source area is conveniently called headwall in this paper as quite often the headwall consists of a major part of the source area. Elevation and slope distributions of the headwalls were calculated from 1 arc-second ASTER Global Digital Elevation Model version 2 (accessed from https://lpdaac.usgs.gov/dataset_discovery/aster/aster_products_table/astgtm).

The distribution of mean annual temperature, T_{ma} (°C), over each of the headwalls was obtained by linearly extrapolating from the nearest location where such data exist, using a constant lapse rate γ (°C/m) (Table S1). For Imj, Khu, and Ngz Glaciers, data from Scherler (2014); for Mil and G2 Glaciers, data from Gurung et al. (2016); for Sat Glacier data from Dobhal et al. (2013); for Bar and Ham Glaciers, data from Azam et al. (2016) were used. The data used for each of the glaciers are listed in Table S1.

As a proxy for avalanche activity on each of these glaciers (Laha et al., 2017), we compute the product of mean Tropical Rainfall Measuring Mission rainfall (Kummerow et al., 1998) at the glacier headwall, and the corresponding ice-free headwall area above a cut-off slope of 30°. The processed 4 km horizontal resolution 2B31 product is made available by Bodo Bookhagen that is accessible from http://www.geog.ucsb.edu/~bodo/TRMM/.

3.1. Supraglacial debris flux

We use available remote-sensing-based debris-thickness distribution data from Imj, Khu, Ngz (Rounce and McKinney, 2014) and Bar Glaciers (Schauwecker et al., 2015). Our data for Ham (Fig. 2) and Sat (Fig. S4) Glaciers are obtained by manual measurements at 121 and 79 pits, respectively, dug on these two glacier surfaces during the period 2014 to 2016.

For each of these six glaciers, multi-annual velocity profiles were obtained using remote-sensing method by Scherler et al. (2011a). The reliability of the remote-sensing velocity measurements was assessed using available field data from Ham Glacier (Shukla et al., 2015). The remotely-sensed velocity profile compares very well with the field measurements of velocity on the same glacier (Fig. S6). In general, there may be differences between our choice of central flowline (Fig. 2a, S4) and that of Scherler et al. (2011a). We have matched the profiles by matching the terminus of the glacier and used the same horizontal axis as

Download English Version:

https://daneshyari.com/en/article/8906743

Download Persian Version:

https://daneshyari.com/article/8906743

Daneshyari.com